Pressure Fluctuations due to 'Trapped Waves' in the Initial Region of High-speed Jets

K.B.M.Q. Zaman[1] and A.F. Fagan[2]
NASA Glenn Research Center
Cleveland, OH 44135

An experimental study was conducted on unsteady pressure fluctuations occurring near the nozzle exit and just outside the shear layer of high-speed jets. These fluctuations are related to 'trapped waves' within the jet potential core as investigated and reported recently by other researchers. Round nozzles of three different diameters and rectangular nozzles of three different aspect ratios are studied. The pressure fluctuations manifest as a series of peaks in the spectra. Usually the first peak at the lowest frequency has the highest amplitude while the amplitude decreases progressively for successive peaks at higher frequencies. These 'trapped wave spectral peaks' are found with all nozzles. Their characteristics and variations with axial and radial distances, jet Mach number as well as aspect ratio of the nozzle are discussed. For round nozzles, the frequency of an individual peak is found to scale with the nozzle diameter; thus, on a Strouhal number versus jet Mach number plot each spectral peak is represented by a unique curve independent of the nozzle diameter. Empirical equations are provided for these curves for the dominant peaks. For rectangular nozzles, the number of peaks observed near the long edge is found to be larger than that observed near the short edge by a factor equal to the nozzle's aspect ratio. The trapped wave spectral peaks continue to persist in the supersonic regime. Intriguingly, the onset of screech tones appears to be a continuation of the evolution of these peaks; it is as if one of these peaks abruptly increases in amplitude and turns into the screech tone as the jet Mach number is increased.

I. Introduction

Recent research based on 'mining' of data from a Large Eddy Simulation (LES) has identified a system of instability waves in round high-subsonic jets that are not the same as the well-known Kelvin-Helmholtz (K-H) waves. These, often referred to as 'trapped waves', are apparently predicted by a second-branch solution of the spatial stability theory for free shear layers. Reference 1 provides a seminal account of the phenomenon. These waves are not detectable in the far-field and hence went unnoticed in the vast literature on jet noise experiments. They have also gone undetected in the vast literature on jet instability and excitation studies apparently because the K-H waves grow fast and dominate the flow field. It is also possible that probe interference such as with hot-wire anemometry alters the trapped waves and renders them difficult to discern.

However, a microphone placed close to the nozzle exit and just outside the shear layer picks up the signature of these waves. Reference 2 is perhaps the first experimental study noting such pressure fluctuations near the edge of a jet. A few of the microphones in a 'phased array' exhibited certain spectral peaks. The authors thought these were spurious and possibly related to facility resonances. They explored the connection of these peaks to upstream duct modes and the results were inconclusive. They narrated their observations in an appendix of the paper. It should be noted that the authors of Ref. 1 also conducted an experiment and observed similar spectral peaks whose frequencies compared well with their LES as well as analytical results.

[1] Inlets & Nozzles Branch.
[2] Optics & Photonics Branch.

Clearly, there should be more than an academic interest to understand these waves. They are an integral part of the jet shear layer instability that in turn dictates the initial development of the jet. Even though these waves are not readily detectable in the far field, it stands to reason that computational fluid dynamics and aero acoustics (CFD and CAA) codes must account for them for accurate prediction of jet noise. Curiously, these waves appear to have some linkage with screech tones since with increasing jet Mach number that certain trapped wave spectral peaks rise in amplitude and seem to turn into the screech tone. This is further explored and discussed. Another possible relevance could be in jet-surface interaction and, therefore, in propulsion/airframe noise. A plate when placed near a rectangular or a round nozzle is found to amplify these spectral peaks and sometimes yield resonant tones. However, this last aspect has remained from being fully explored and will not be addressed further in this paper.

The present experimental study is undertaken to explore further details of the unsteady pressure fluctuations near the exits of a variety of nozzles. Following Ref. 1, such fluctuations will be simply referred to as 'trapped waves' and the corresponding spectral peaks in the pressure signal as 'trapped wave spectral peaks'. Using a single microphone the pressure spectra are measured for varying streamwise and radial distances as well as for varying jet Mach number. This is carried out for round nozzles of different diameters as well as for rectangular nozzles of different aspect ratios. Preliminary data have been documented in a NASA technical memorandum [3]. Those and further results from the continuing investigation are discussed in this paper. Key findings are described with observations simply from an experimentalist's vantage point without any attempt to relate them to analytical results, e.g., discussed in Ref. 1.

II. Experimental Facility

The experiments are conducted in an open jet facility at NASA GRC. Compressed air passes through a 30″ diameter plenum chamber before exhausting through the nozzle into the ambient of the test chamber. An interested reader may find further description of the facility in earlier publications, e.g., [4, 5]. The pressure fluctuation spectra are measured by a microphone (¼-in, B&K 4135) mounted on a probe traversing mechanism. All spectral data presented in the following are taken with the ¼-in microphone. As described with the results, for spatial resolution concerns a 1/8-in microphone is also used to repeat some data for a small nozzle. Limited far-field noise data, taken with a fixed microphone, are discussed. Data acquisition is done using a National Instruments A/D card and Labview™ software. Spectral analysis is done typically over 0-50kHz with a bandwidth of 50 Hz, using a data rate of 100 kHz and a 50 kHz low-pass filter. For larger nozzles the analysis range is sometimes reduced with a correspondingly shorter bandwidth, so that the spectral peaks are captured with adequate resolution.

Figure 1 shows pictures of various nozzle configurations. All nozzles are convergent. The one in Fig. 1(a) is the 'SMC000' case (small metallic chevron nozzle; without chevrons) that will be referred to simply as 'SMC' in the following. It is attached to the plenum chamber through adapters having smooth, converging interior contours. This round nozzle with exit diameter of 2″ has been used previously in several experimental as well as numerical studies; Ref. 4 cites a few such previous and ongoing works. All dimensions are given in inches.

The configuration shown in Fig. 1(b) involves the SMC nozzle with a 12″ long upstream pipe. It has been shown to generate a fully turbulent exit boundary layer whereas without the pipe the nozzle has a 'nominally laminar' boundary layer [4]. Figures 1(c) and 1(d) show a 1″ and a 0.58″ diameter round nozzle, respectively. While the exit boundary layers for the smaller nozzles have not been measured they are also likely to be nominally laminar. Figure 1(e) shows a 2:1 aspect ratio rectangular nozzle with the long edge placed horizontally. Figure 1(f) shows an 8:1 aspect ratio nozzle with the long edge placed vertically. In most of the pictures the microphone used for the measurements can be seen. Not shown is a 4:1 rectangular nozzle, also used in the experiment. All three rectangular cases have an equivalent diameter of 2.12″ based on the exit area; further descriptions including exit boundary layer data can be found in [5].

The 'jet Mach number' M_J is used as an independent variable. It is defined based on the plenum pressure, p_0, and the ambient pressure, p_a, and given by, $M_J = (((p_0 / p_a)^{(\gamma-1)/\gamma} - 1)\frac{2}{\gamma - 1})^{1/2}$, where γ is the ratio of specific heats for air. Note that in supersonic conditions, it is fictitious and represents the Mach number had the flow expanded fully. All data reported are for cold flows, i.e., with the total temperature the same everywhere as in the ambient.

III. Results and Discussion

Round nozzle data: Pressure fluctuation spectra measured near the exit of the SMC nozzle are shown in Fig. 2(a) for varying streamwise distance (x) with a fixed radial distance (r=0.75); here, the distances are nondimensionalized by the nozzle diameter (2″). The coordinate origin is located at the center of the nozzle exit. The ordinate in Fig. 2(a) pertains to the trace at the bottom (x=0) and successive traces are staggered by 10dB. A series of peaks mark the spectra especially near the nozzle exit for the given r. These are similar to those reported in Refs. 1 and 2. Away from the exit the spectral peaks get buried under broadband turbulence apparently when the microphone begins to encounter some flow. In Fig. 2(b) corresponding data are shown for a fixed x but for varying r. When the microphone is too close to the jet (r=0.6), it encounters flow resulting in a broadband peak, in this case, centered around 12 kHz. The spectral peaks are seen to diminish in amplitude with increasing radial distance.

Corresponding data for varying jet Mach number (M_J) at a point near the nozzle exit (x=0.2, r=0.75) are shown in Fig. 3(a). The trapped wave spectral peaks are not clearly visible at the lowest M_J (=0.548) but they become prominent with increasing value of M_J. The frequency of a given spectral peak decreases with increasing M_J. Such a behavior was also noted in Ref. 2 leading to the inference that these peaks do not follow a Strouhal number scaling; (if the Strouhal number based on nozzle diameter remained constant, the frequencies would have increased with increasing M_J). This point is addressed further later. In Fig. 3(b) corresponding sound pressure level spectra in the 'far-field' are shown; the microphone location is 25D from the jet exit and at a polar angle of 60° relative to the jet axis (the location is shown schematically with inserts in some figures to aid the reader). The trapped wave spectral peaks are known to be undetectable in the far-field noise spectra. Here, some undulations (marked by the arrows) especially at higher M_J conditions can be noticed that appear to be the footprint of the trapped waves. It is possible this is because 25D distance is still not the far acoustic field. Also, the experimental arrangement is not anechoic and there are some uncovered reflecting surfaces in the vicinity of the nozzle (e.g., the probe traversing mechanism, flanges etc.).

Figure 4 shows pairs of spectral data at three values of M_J. These data are for the SMC nozzle with one set taken with the upstream pipe (Fig. 1b) and the other without the pipe (Fig. 1a). Through hot-wire measurements it was shown earlier in Ref. 4 that the nozzle with the pipe involves a fully turbulent exit boundary layer whereas the case without the pipe involves a 'nominally laminar' boundary layer. (In the latter case the mean velocity profile has a shape similar to that of a 'Blasius-profile' characteristic of laminar boundary layer but involves large fluctuation intensities. The former case involves a slow decay of mean velocity as the nozzle wall is approached with turbulent fluctuations penetrating far from the wall. The momentum thickness in the former case is about three times larger than that in the latter case). The nearly congruent traces in each pair (Fig. 4) indicate that the trapped waves are not influenced by the exit boundary layer (BL) characteristics. It is apparent that the trapped wave spectral peaks also do not scale on the exit BL thickness for a given boundary layer state (laminar or turbulent); BL thickness decreases with increasing M_J, so a Strouhal number based on the thickness would not remain constant and in fact decrease more rapidly with increasing M_J. The frequency scaling is discussed further in the following. One other point is note-

worthy. Figure 4 includes a set of data at a supersonic condition where screech has ensued (represented by the tall peak in the spectra which manifests as an audible tone). The progression of the spectral peaks with increasing M_J suggests that one of the trapped wave peaks has turned into the screech component. This point is also addressed further in the following.

Figure 5(a) shows data from the 1″ diameter jet with varying *x*, similarly as done in Fig. 2(a) for the 2″ jet. Very similar trends are noted except that the frequencies of the peaks are higher; this is analyzed further shortly. The same comment can be made for radial variation of the spectra shown in Fig. 5(b). Likewise, a similar trend is observed for jet Mach number variation, shown in Fig. 6(a). In Fig. 6(b) data for the 1″ diameter nozzle are shown in the supersonic regime. In the range $M_J \geq 1.083$ there is screech. With increasing M_J the screech frequency decreases and there is a 'stage jump' around M_J =1.2. An inspection again reveals a continuous trend. It is as if the screech component locks on to one of the trapped wave spectral peaks. With increasing M_J, it first locks on to the third peak (clearly at M_J = 1.117) and after the stage jump it locks on to the second peak. Throughout the entire M_J range covered, the frequency of an individual peak decreases with increasing M_J.

Data for the smallest (0.58" diameter) nozzle is shown only for variation of M_J, in Fig. 7. These data are measured by the ¼-in microphone which is relatively large. A 1/8-in microphone is used to cross-check and the spectral peaks are found to repeat well (not shown for brevity). Comparing the data in Figs. 3(a), 6(a) and 7, a consistent increase in the frequencies of the trapped wave peaks is noted with decreasing nozzle diameter. This is examined in Fig. 8 where data for all three nozzles are plotted as a function of Strouhal number based on the diameter; (jet velocity, defined to be equal to M_J times the ambient speed of sound, is used for velocity scale). Two sets of data are shown for M_J =0.92 and 1.01, as examples, in Figs. 8(a) and (b), respectively. The trapped wave spectral peaks are found to be approximately congruent for the three nozzles with different diameters. A scrutiny also reveals that the spectral peaks are not direct harmonics. For example, the first three peaks for M_J =0.91 occur at Strouhal numbers 0.377, 0.624 and 0.879; those for M_J =1.01 occur at 0.345, 0.576 and 0.808. However, there might be an integral relationship. Note that the ratio of the second and first numbers (0.624/0.377) is about 5/3 while that of the third and the second numbers (0.879/0.624) is about 7/5. The same ratios hold true for the Strouhal numbers at the higher M_J. See further discussion at the end of this subsection.

The Strouhal numbers of the four tallest peaks in each spectra (usually the four from the left at low frequencies) are plotted in Fig. 9. The symbol size (and shape) are varied according to the amplitude; circles represent the highest while the square, diamond and delta shapes represent the lower amplitudes in decreasing order. Note also that red, blue and green symbols represent the 2″, 1″ and 0.58″ nozzles, respectively. An interesting trend emerges. The trapped wave spectral peaks follow distinct branches. Generally, the amplitudes are the highest at the lowest branch and decrease at the upper branches. However, screech, representing the tallest peak in the supersonic regime, often locks on to the peaks in the upper branches. Screech seems to blend with the family of curves quite well. This is further scrutinized with data from the SMC nozzle and a rectangular nozzle in the following.

It is apparent that the trapped wave spectral peaks follow a Strouhal number scaling after all (based on nozzle diameter). However, the Strouhal number is not a constant and it is a distinct function of M_J in each of the branches. The data on exit BL effect (Fig. 4) and for nozzles of different diameters (Figs. 8 and 9) strongly suggest that the spectral peaks do not scale on the initial shear layer (exit BL) thickness. Had the ratio of the thickness to diameter remained constant for all nozzles scaling on the diameter would be equivalent to scaling on the exit BL thickness. Although it has not been measured, that ratio is unlikely to be the same for all three nozzles. Furthermore there is the stark contrast in BL thickness in Fig. 4 that has practically no effect on the spectral peaks. In Fig. 9 if the data were nondimensionalized by exit BL thickness instead of diameter they would not fall on a single curve for each branch. Thus, it is safe to infer that the trapped wave spectral peaks do not scale on initial shear layer thickness, contrasting the characteristics of K-H waves.

The data in Fig. 9 provide an engineering correlation for prediction of the trapped wave frequencies for round nozzles. For a given diameter, the frequencies can be calculated using empirical curves fitted through each branch. Curves of the shape, $St=M_J^{-A}+B$, are fitted where St is the Strouhal number (ordinate in Fig. 9). The fitted curves are shown by the lines in Fig. 9. The coefficients (A, B) for the four branches are as follows: (fit 1: 0.7169, -0.6745), (fit 2: 1.0926, -0.4642), (fit 3: 1.4260, -0.2578) and (fit 4: 1.6728, -0.0211). With reference to the discussion regarding an integral relationship among the frequencies of the spectral peaks in Fig. 8, and with the peaks denoted as f_1, f_2, f_3, etc. with increasing frequency, the following relationships appear to hold: $f_2=(5/3)f_1$, $f_3=(7/5)f2=(7/3)f_1$, etc. That is, $f_n=((2n+1)/3)f_1$. The implication of this as to the origin of the trapped wave peaks remains unexplored at the present time.

Rectangular nozzle data: The data so far pertained to round nozzles. The behavior of near-exit pressure fluctuations was then explored for rectangular nozzles. The nozzles were readily available and the explorations could be extended with the same facility and instrumentation. With a rectangular nozzle the widths in the major and the minor axis directions present two length scales. The occurrence of the trapped waves is investigated on both the short and the long edges. Microphone locations nondimensionalized by the equivalent diameter (D_{eq} = 2.12″) are indicated in the captions of the following figures; coordinates *y* and *z* denote the vertical and horizontal distances from jet axis, respectively, while *x* denotes the axial distance from the nozzle exit.

Figure 10 shows the spectral traces with varying M_J for the 2:1 rectangular nozzle (exit: 1.328″x2.665″) with the microphone placed on the major axis, i.e., near the short edge. For convenience, the microphone location is shown schematically with the insert. Obviously, the trapped waves are also detected with the rectangular nozzle! The trends are similar to that seen with round nozzles: they occur above a certain M_J and the frequencies of individual peaks decrease with increasing M_J. It will be shown next that the number of spectral peaks here depend on the side of the nozzle where the microphone is placed.

Data on the major axis versus the minor axis (short edge versus long edge) of the 2:1 case are compared in Fig. 11(a) for M_J =0.91. The trapped waves are also detected on the long edge, however, the peaks occur less frequently, coinciding approximately with every other peak seen on the short edge. Note that the microphone orientation relative to the edge of the nozzle is different for the two cases in Fig. 11(a). That this did not cause a difference in the spectra is checked by another set of data taken with the nozzle rotated by 90°, shown in Fig. 11(b). The difference in the number of trapped wave spectral peaks on the long and short edges are further documented in Fig. 12 for two other values of M_J. The number of peaks seen on the long edge (minor axis) are approximately one-half of those seen on the short edge. The first (dominant) peak is seen on both edges but only the third and fifth seen on the short edge approximately coincide with the second and third seen on the long edge, respectively; at higher frequencies the amplitudes are small and there is increasing randomness in such matching.

Corresponding data with varying M_J for the 4:1 aspect ratio case (exit: 0.940″x3.765″) on the short edge are shown in Fig. 13(a). The trapped wave peaks are again present, however, they are tightly packed. On the other hand, as shown in Fig. 13(b), on the long edge the peaks are dispersed and not as sharp. An inspection suggests that the number of peaks on the long edge here are approximately 4 times less than those seen on the short edge.

The trend continues for the 8:1 aspect ratio nozzle (exit: 0.661″x5.340″) as shown in Fig. 14. On the short edge the peaks are more tightly spaced (Fig. 14a). The number of peaks on the long edge appear to be approximately 8 times less than that seen on the short edge (Fig. 14b). The 'long wavelengths' (wider spacing of the peaks) noted on the long edge are not affected by microphone orientation (Fig. 14c). The wider spacings of the peaks are observed over the entire span and even near the corner of the nozzle (Fig. 14d). Therefore, the ratio of the number of peaks seen on the long and short edges appear to be simply dictated by the aspect ratio. It is as if a lateral resonance in the major axis direction is detected on the minor axis location and vice versa.

Further data on screech tones: An apparent and intriguing linkage of the trapped wave spectral peaks with screech tones was noted in discussing figures 4, 6 and 9. This was further explored with the SMC and the 2:1 rectangular nozzle. Near-field spectral data for the SMC nozzle are shown in Fig. 15 for increase in M_J at small increments. For clarity the data are split into two figures for lower and higher M_J ranges. As noted earlier, with increasing M_J the third trapped wave spectral peak is seen to amplify and apparently turn into screech (Fig. 15a). From past knowledge, and the value of M_J, this is the A1 mode of screech [7-9]. With further increase in M_J the frequency decreases and the pattern appears to be a continuation of the trend noted for the branches of trapped waves seen in subsonic conditions. However, the rate of decrease in screech frequency appears to be more than that seen at lower values of M_J when screech has not yet ensued. Figure 15(b) is a continuation of the data with further increase in M_J when there is a stage jump and the second trapped wave peak becomes the screech tone for M_J >1.268. Essentially the same observation was made with the 1" round nozzle in Fig. 6(b).

A similar trend is observed also with the 2:1 rectangular nozzle, as shown in Fig. 16. Data taken on the minor axis (near the long edge) is shown in Fig. 16(a). With increasing M_J here it appears that the second trapped wave peak turns into the screech tone. However, recall that the number of spectral peaks is twice on the major axis (near the short edge). Thus, it is the third trapped wave peak that turns into the screech tone when viewed on the major axis location (Fig. 16b). Thus, for the rectangular jet the onset of screech tones also appears to be a continuation of the trapped waves with increasing M_J. (This could not be checked with the other two rectangular nozzles because of the interruptions due to COVID19 crisis; hopefully such data will be in hand for a possible Journal submission of the manuscript based on these results).

Recall that with the SMC nozzle the onset of screech was a continuation of the third trapped wave peak, however, there was a lack of continuity in the subsequent rate of change in frequency with increasing M_J (Fig. 15a). This is examined in the contour plot of Fig. 17 based on spectral data from the fixed near field microphone. The plot covers a wider range of M_J based on 47 spectral traces, including the ones covered in Fig. 15. On the left (Fig. 17) in the subsonic regime the branches of trapped waves can be seen clearly; the dashed lines are the empirical fits discussed with Fig. 9. In the supersonic regime, screech tones are represented by the regions of high amplitudes (red). Well-known screech stages (A1, A2, B, C and D) are marked in the plot (following observations in references, e.g., [7-9]). (Note that M_J -ranges for these stages vary somewhat from nozzle to nozzle and facility to facility; also, sometimes other stages pop up such as a B' stage noted in [9]). The upper two bands of deep red on the right are due to the first harmonics of the B and D stages.

It becomes apparent that the A1 and A2 stages approximately match the general continuation of the third branch of the trapped waves, while B and D stages coincide with the continuation of the second branch. However, the screech bands exhibit some departures from the trends of the trapped wave branches. For example, the A1 and A2 stages do not exactly match the fitted curve for branch 3. Stage C stands out and does not fit any of the branches. Nonetheless, that the onset of screech for both the circular and the rectangular nozzle occurs as a continuation of the trapped wave branches is almost unmistakable. This may lead one to speculate that the morphology of screech and the trapped waves trace to similar mechanisms. However, this is purely an experimental observation without any theoretical basis at this time.

IV. Conclusions

Near the nozzle exit and around the edge of high-speed jets unsteady pressure fluctuations are observed that manifest as a series of peaks in the spectrum. These are the footprints of 'trapped waves' within the potential core of the jet as revealed by recent research based on LES data mining as well as analytical studies. In this experimental study the characteristics of the spectral peaks are explored for a set of round nozzles of different diameters as well as a set of rectangular nozzles of different aspect ratios. In all cases,

the frequency of the spectral peaks is found to decrease with increasing jet Mach number. For the round nozzles it is shown that the spectral peaks remain unaffected by the exit BL state and thickness. The frequencies are found to scale on the jet diameter. The Strouhal numbers based on the diameter for all nozzles are found to follow distinct branches of a family of curves when plotted as a function of M_J. This provides an engineering correlation for prediction of the frequencies. Curve-fit equations are provided for this purpose for the four most dominant spectral peaks.

With the rectangular nozzles the trapped wave spectral peaks are also observed. However, the frequencies of the peaks depend on the observation location. More tightly packed spectral peaks occur on the short edge while the peaks are dispersed on the long edge. The ratio of the frequencies of the peaks on the short and long edge is found to be close to the aspect ratio of the nozzle.

With increasing jet Mach number the onset of screech is noted to occur on a continuation of the trapped wave branches. It is as if one of the trapped wave spectral peaks gets amplified and turns into the screech component. For the round nozzle as well as the 2:1 rectangular nozzle it is the third branch of the trapped waves that first turn into screech. With further increase in M_J there is a stage jump when the screech component matches with the continuation of the second branch of the trapped waves. This is an experimental observation without any theoretical support at this time.

Acknowledgement

The first author wishes to thank Dr. Aaron Towne (Ref. 1) for a discussion of the topic at the AIAA/CEAS Aeroacoustics Meeting in May, 2019 that inspired the present experimental effort. Thanks are also due to Prof. Christopher Tam whose analytical work (Ref. 6) inspired the experiments with the rectangular nozzles, to Dr. Puja Upadhyay for help in various forms throughout the study, and to Dr. Christopher Miller for pointing out the apparent integral relationships among the frequencies of the spectral peaks. This work is supported by NASA's Commercial Supersonic Technologies (CST) and Transformational Tools and Technologies (TTT) Projects.

References

[1] Towne, A., Cavalieri, A.V.G., Jordan, P. Colonius, T., Schmidt, O., Jaunet, V. and Brès, G.A., "Acoustic resonance in the potential core of subsonic jets", *J. Fluid Mech*., vol. 825, pp. 1113-1152, doi:10.1017/jfm.2017.346, 2017.

[2] Suzuki, T. & Colonius, T., "Instability waves in a subsonic round jet detected using a near-field phased microphone array", *J. Fluid Mech*., vol. 565, 197–226, 2006.

[3] Zaman, K.B.M.Q., "Near-exit pressure fluctuations in jets from circular and rectangular nozzles", *NASA/TM*—2019-220383, November 2019.

[4] Zaman, K.B.M.Q., "Exit Boundary Layer Data for a Round Convergent Nozzle in Support of Numerical Simulation Efforts", *NASA/TM*—2019-220242, July 2019.

[5] Zaman, K.B.M.Q., "Flow field surveys for rectangular nozzles", *NASA TM* 2012-217410 (with electronic data files), April, 2012.

[6] Tam, C. and Chandramouli, S., "Jet-plate interaction tones relevant to over-the-wing engine mount concept", *AIAA Paper* 2019-2430, AIAA/CEAS Aeroacoustics Conference, May 20-23, 2019, Delft, Netherlands, 2019.

[7] Norum, T.D., "Control of jet shock associated noise by a reflector", *AIAA Paper 84-2279*, AIAA 9th Aeroacoustics Conference, Williamsburg, VA, 1984.

[8] Zaman, K.B.M.Q., "Spreading characteristics of compressible jets from nozzles of various geometries", *J. Fluid Mech., 383,* pp. 197-228, 1999.

[9] Clem, M.M., Zaman, K.B.M.Q., and Fagan, A.F., "Variation of shock-spacing during screech stage-jumps," *International Journal of Aeroacoustics*, 2016, doi: 10.1177/1475472X16630888.

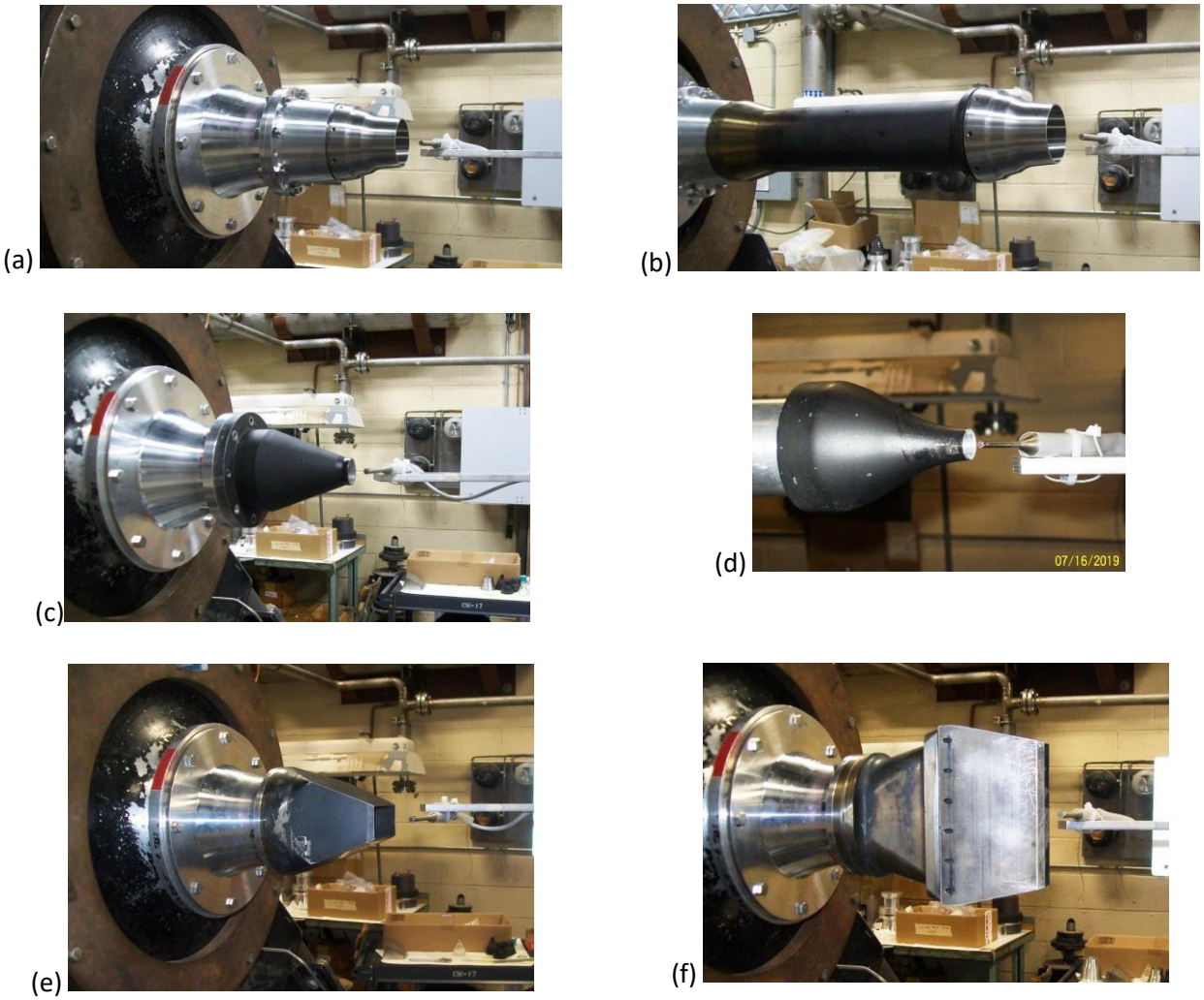

Fig. 1 Nozzle configurations. (a) *D*=2″ ('SMC') nozzle, (b) SMC nozzle with an upstream pipe, (c) *D*=1″ nozzle, (d) *D*=0.58″ nozzle, (e) 2:1 rectangular nozzle, (f) 8:1 rectangular nozzle.

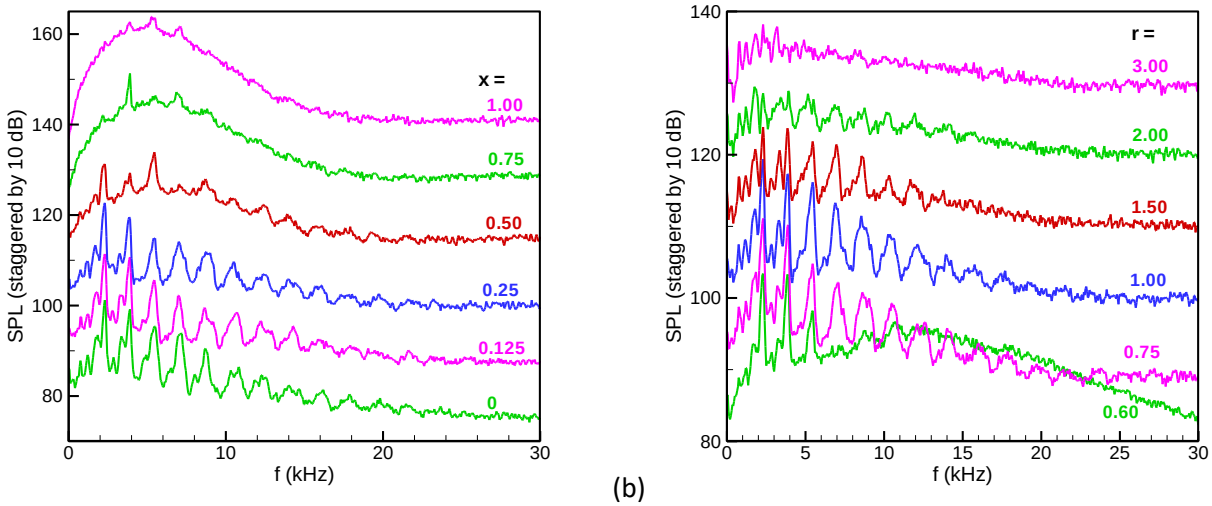

(a) (b)

Fig. 2 Pressure spectra near the exit of the SMC (D=2″) nozzle; M_J =0.91. (a) Varying x at fixed r=0.75, (b) varying r at fixed x=0.2. (Distances normalized by D).

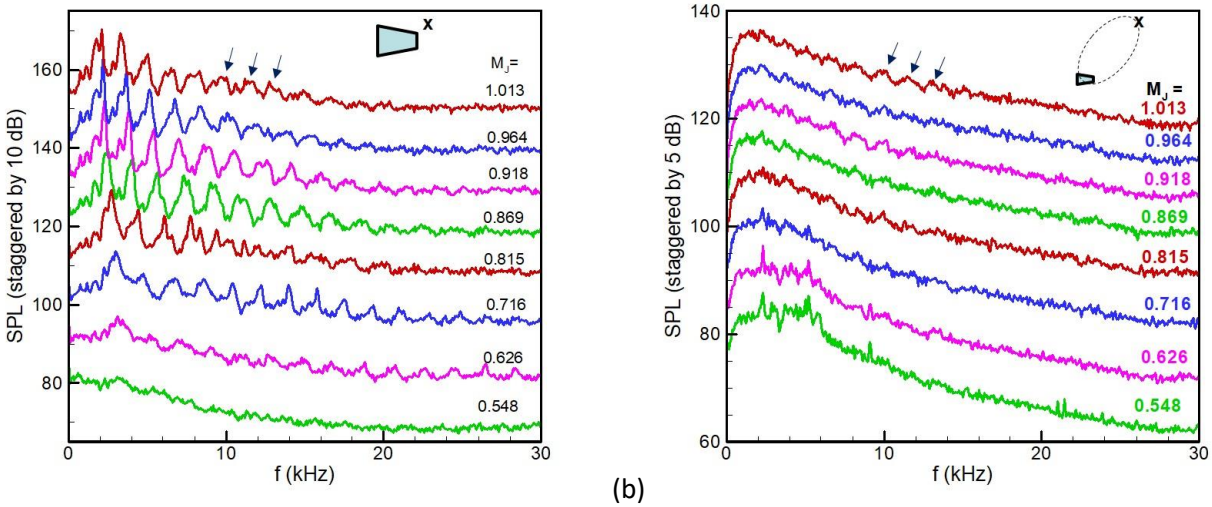

(a) (b)

Fig. 3 Pressure spectra near and far from the SMC nozzle with varying M_J. (a) Near-exit at x=0.2, r=0.75, (b) 25D away from the exit at 60° polar location relative to jet axis.

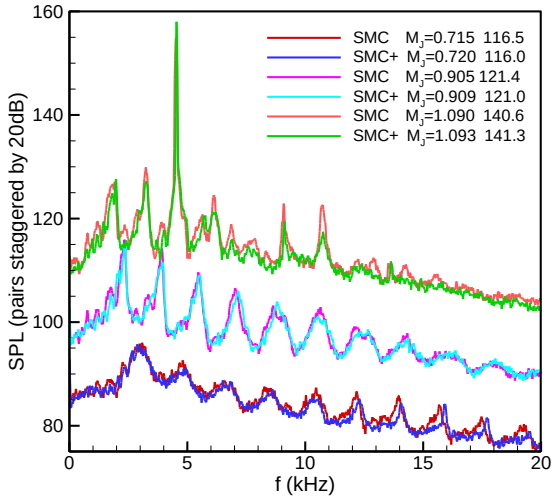

Fig. 4 Pressure spectra at x=0.2 and r=0.75 for the SMC nozzle with and without the upstream pipe. SMC+ denotes the pipe case (see Fig. 1b). The three pairs are staggered successively by 10 dB.

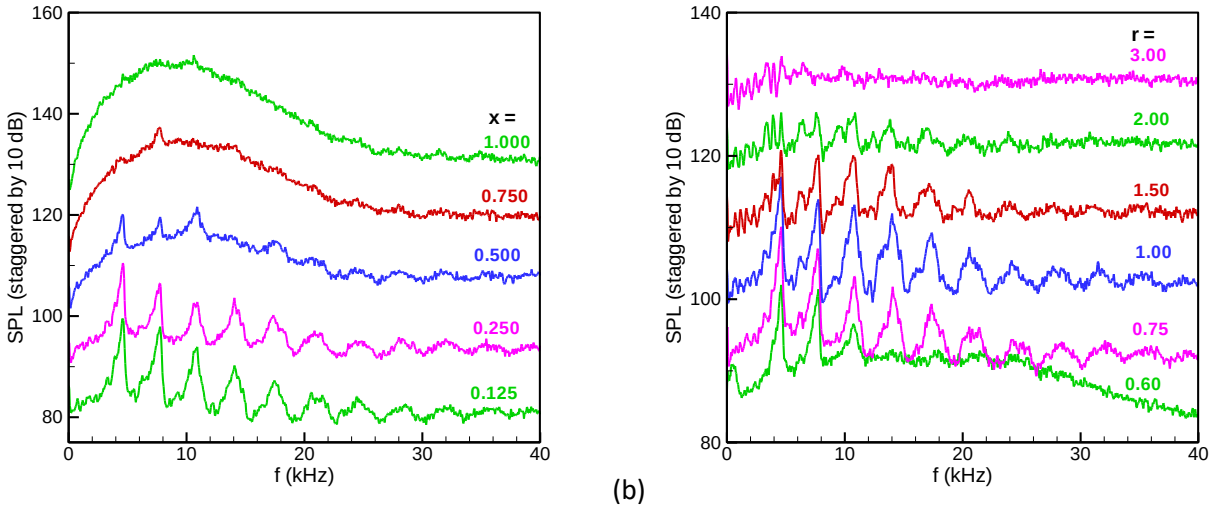

(a) (b)

Fig. 5 Pressure spectra near the exit of D=1″ nozzle for M_J =0.91. (a) Varying x at fixed r=0.75, (b) varying r at fixed x=0.2.

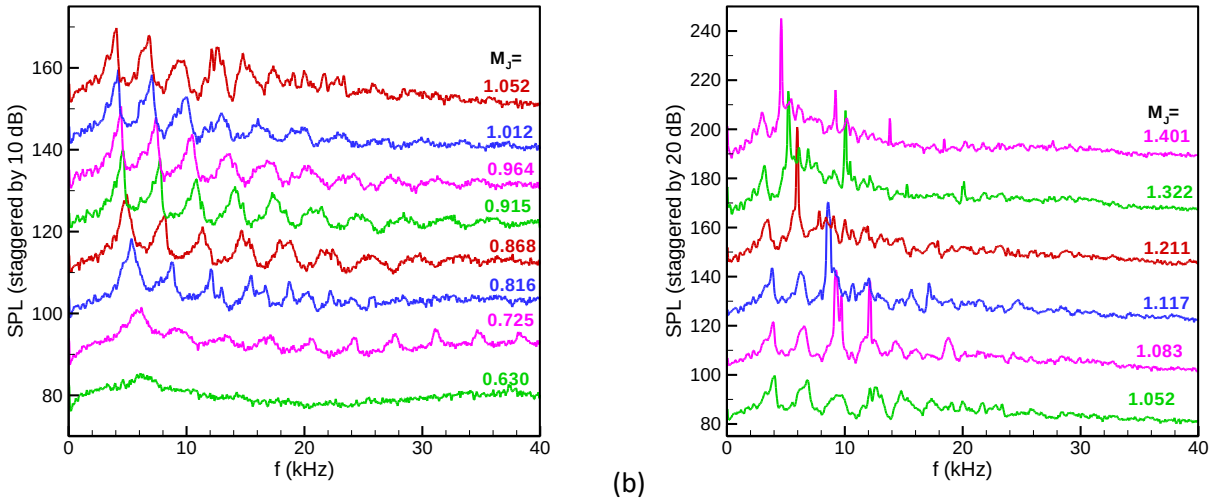

Fig. 6 Pressure spectra for D=1″ jet with varying M_J; x=0.2, r=0.75. (a) Low Mach number range, (b) supersonic range.

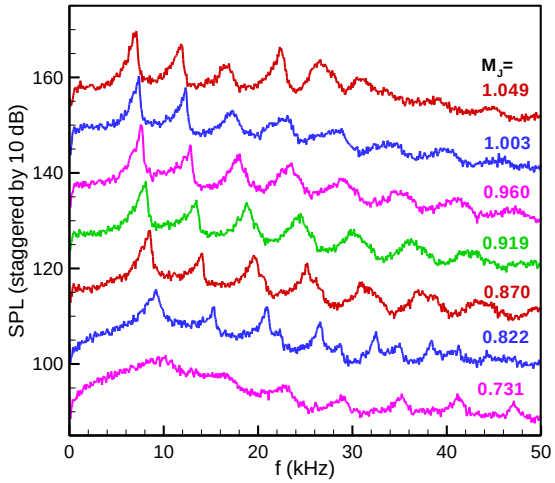

Fig. 7 Pressure spectra for D=0.58″ jet with varying M_J; x=0.2, r=0.75.

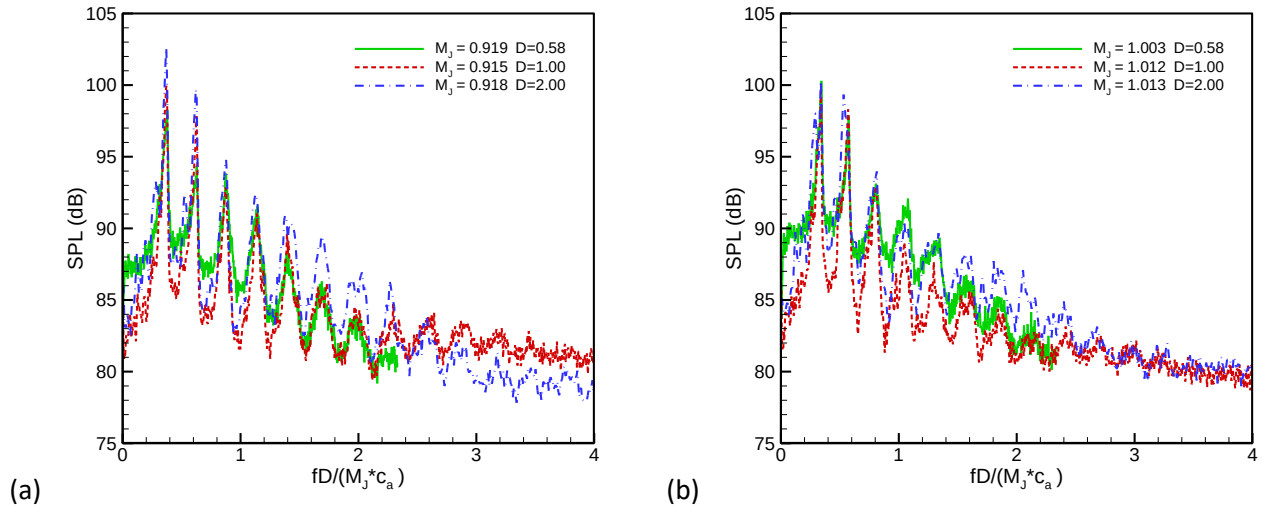

Fig. 8 Pressure spectra for the three round nozzles shown as a function of Strouhal number based on diameter; x=0.2, r=0.75. (a) $M_J \approx 0.91$, (b) $M_J \approx 1.01$.

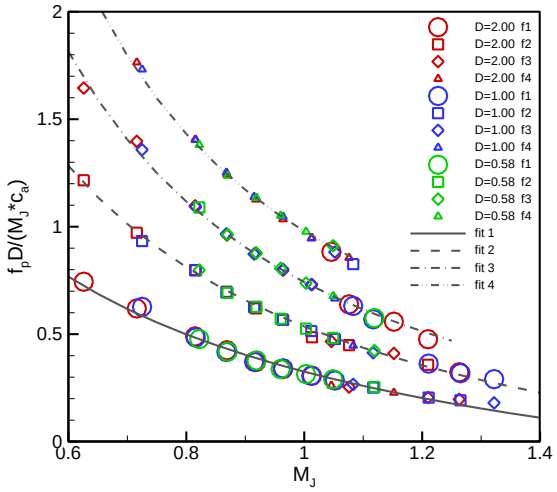

Fig. 9 Strouhal numbers of the four tallest spectral peaks, cross-plotted from data of Figs. 3a, 7a and 8 for the three round nozzle cases. Equations for fitted curves given in the text.

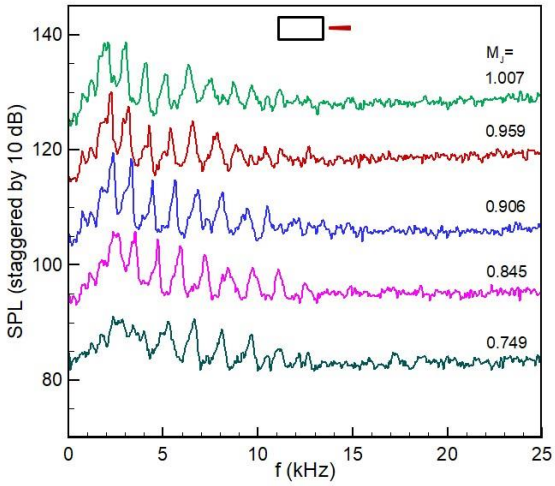

Fig. 10 Pressure spectra for the 2:1 aspect ratio rectangular nozzle with varying M_J; mic on short edge (major axis) at y=0.943, z=0 and x=0.236. (Distances normalized by D_{eq}=2.12″).

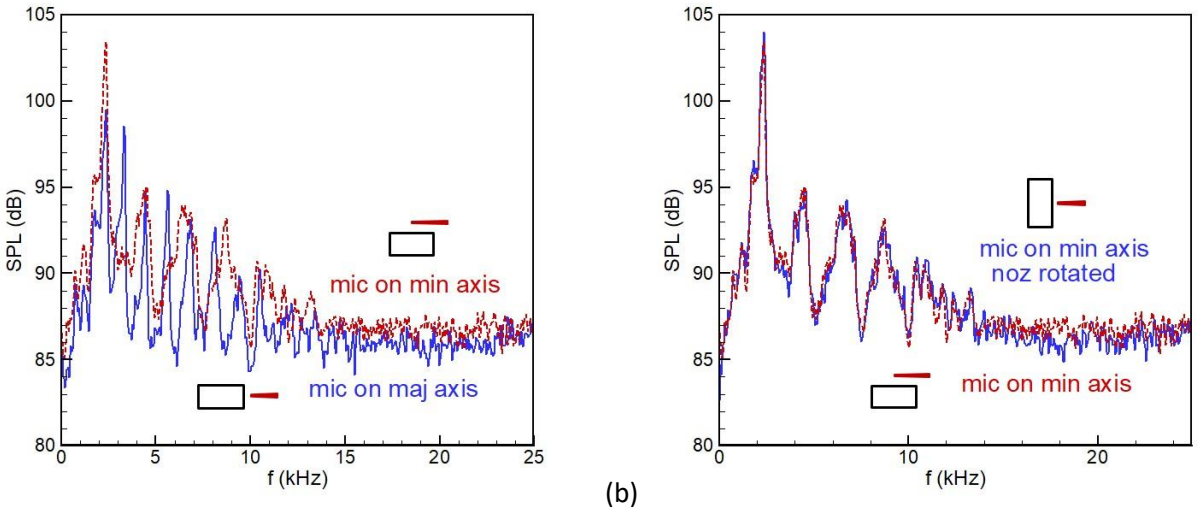

(a) (b)

Fig. 11 Pressure spectra for the 2:1 rectangular nozzle, M_J =0.91, x=0.236. (a) mic on long edge (minor axis) versus short edge (major axis), (b) data on short edge with two relative mic orientation. (Locations for 'Maj axis': y=0.943, z=0; 'min axis': y=0, z=0.637; 'min axis noz rotated': y=0.637, z=0.)

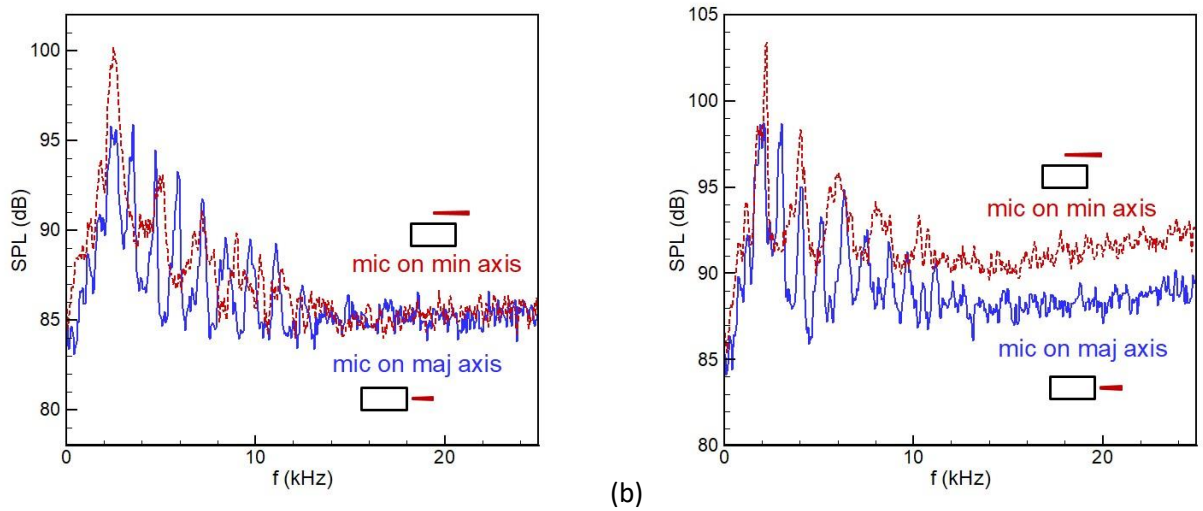

Fig. 12 Pressure spectra for the 2:1 rectangular nozzle with mic on short edge versus long edge for two other values of M_J (mic locations given in Fig 12 caption). (a) M_J =0.845, (b) M_J =1.007.

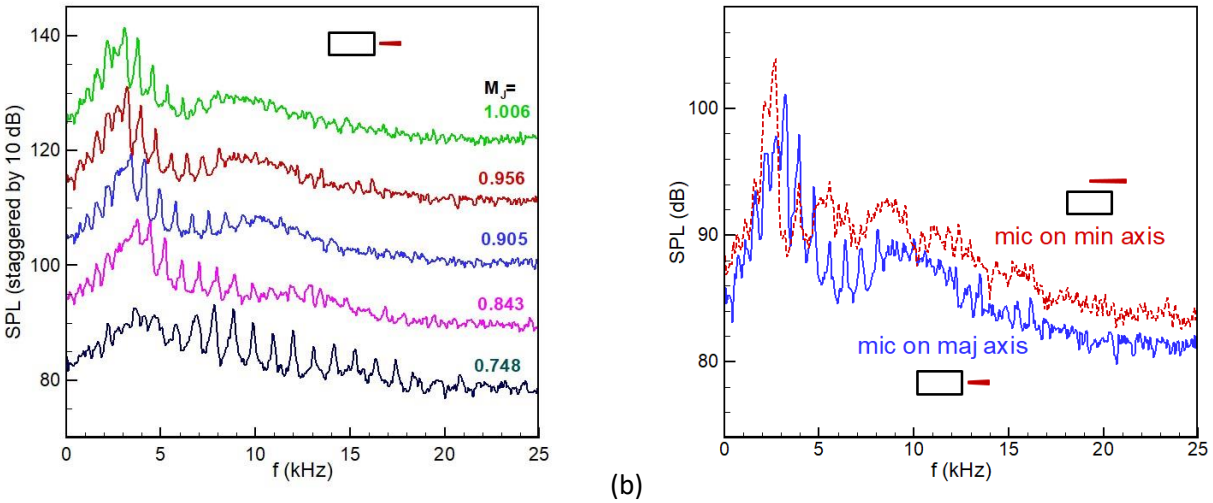

Fig. 13 Pressure spectra for the 4:1 aspect ratio rectangular nozzle, x=0.189. (a) Varying M_J with mic on short edge (y=1.108, z=0); (b) for M_J =0.91 with mic on short edge (y=1.108, z=0) versus long edge (y=0, z=0.443).

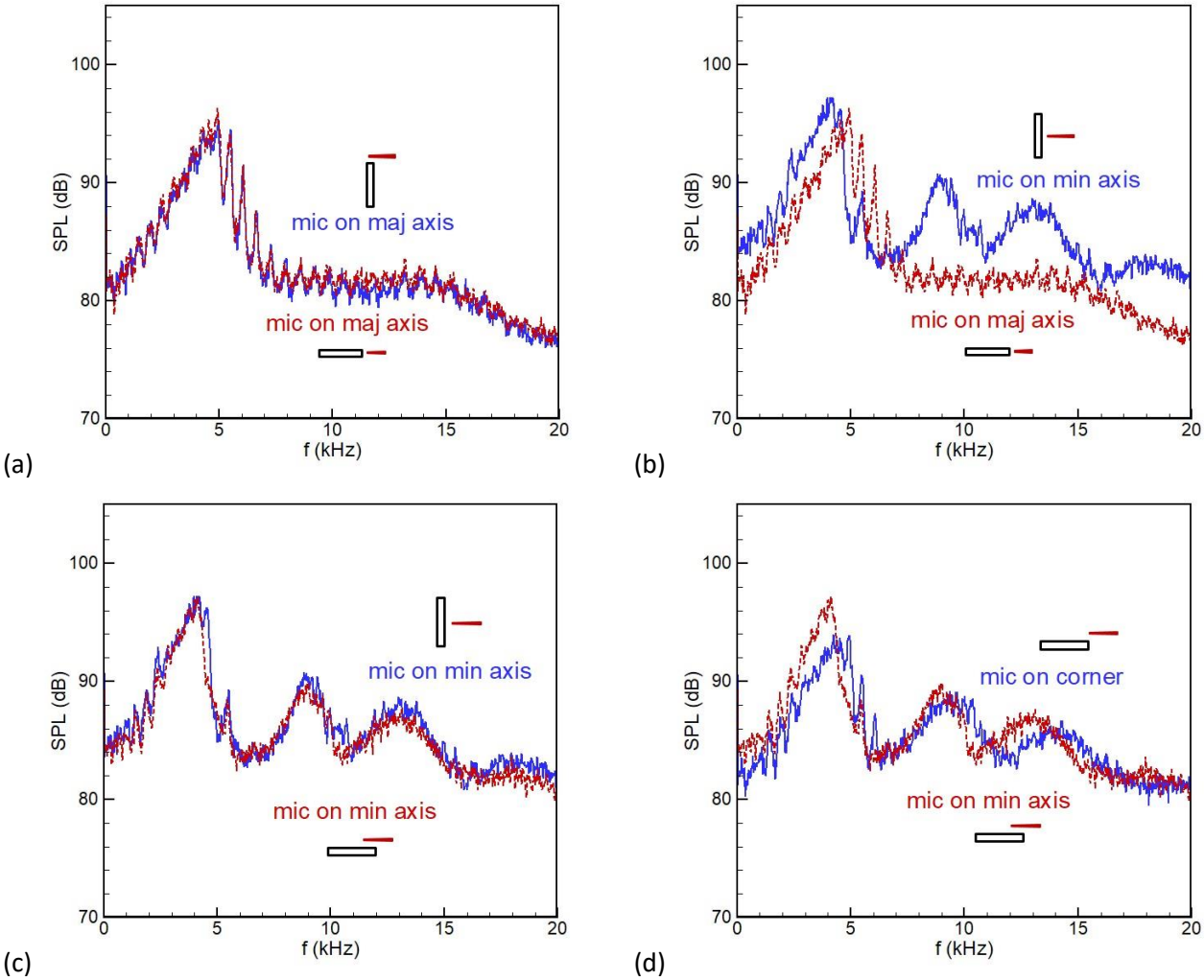

Fig. 14 Pressure spectra for the 8:1 aspect ratio rectangular nozzle at M_J =0.91, x=0.156. (a) Data on short edge with two mic orientation (y=0, z=1.42 and y=1.42, z=0); (b) data on short edge versus long edge (y=0.31, z=0 and y=1.42, z=0); (c) data on short edge with two mic orientation (y=0.31, z=0 and y=0.63, z=0.31); (d) data on short edge at two lateral locations (y=1.26, z=0.31 and y=0.63, z=0.31).

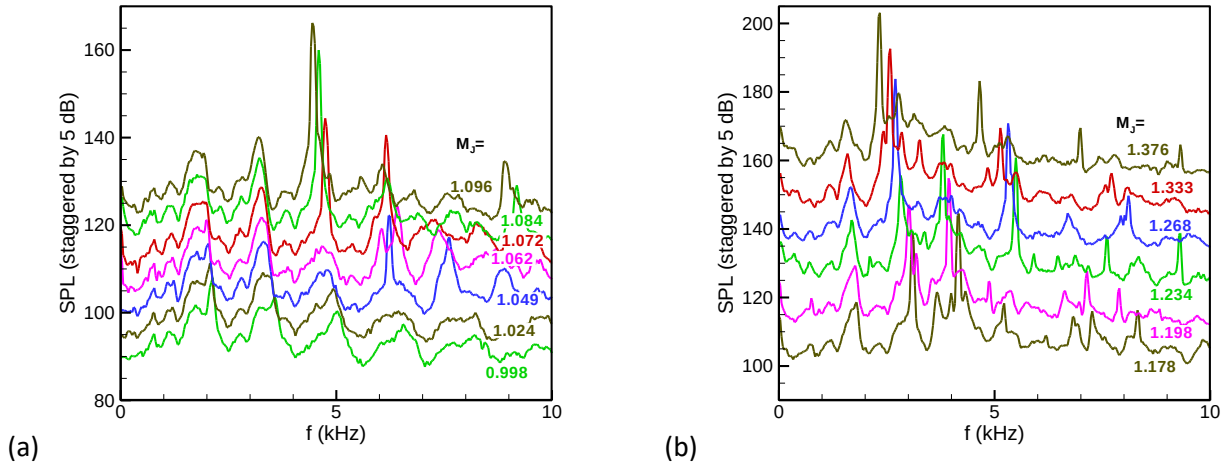

(a) (b)

Fig. 15 Pressure spectra near the SMC nozzle at x=0.2, r=0.75, with varying M_J. (a) M_J-range 0.998-1.096, (b) M_J-range 1.178-1.376.

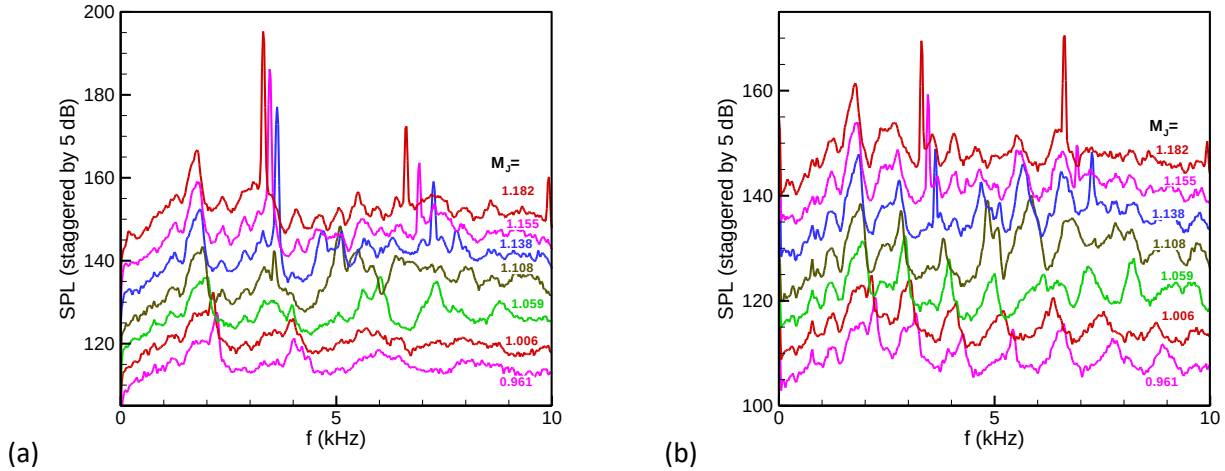

(a) (b)

Fig. 16 Pressure spectra near the 2:1 rectangular jet with varying M_J showing onset of screech tone. (a) Microphone near short edge (y=0.943, z=0, x=0.236), (b) Microphone near long edge (y=0, z=0.637, x=0.236).

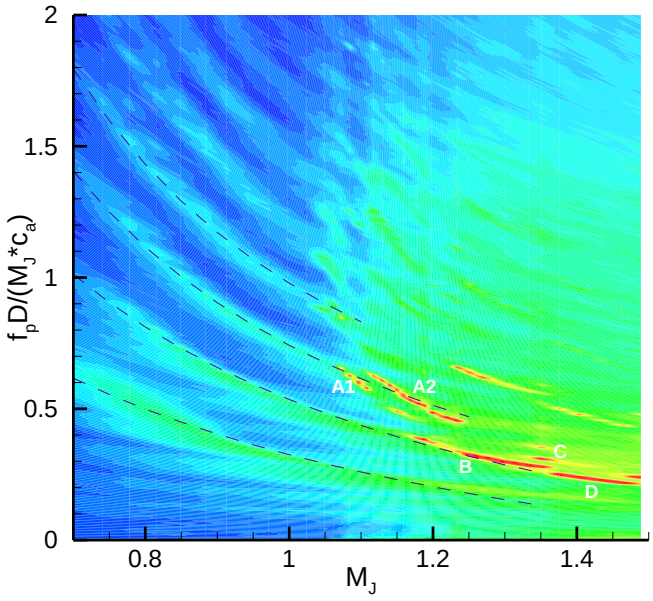

Fig. 17 Contour plot of SPL spectral amplitudes taken with the SMC nozzle at small intervals of M_J (Microphone at x=0.2, r=0.75). Main screech stages are identified. Four dashed curves are empirical fits as in Fig. 9.